

One-Step Fabrication of Silver Nanostructures Decorated Cu-Grid as an Ideal SERS Platform

Menekşe Şakir^{1*} 

¹ ERNAM- Erciyes University Nanotechnology Application and Research Center, Kayseri 38039, Türkiye

*meneksesarihan@erciyes.edu.tr

* Orcid: 0000-0003-3102-0947

Received: 15 February 2023

Accepted: 12 March 2023

DOI: 10.18466/cbayarfbe.1170104

Abstract

Many ways to produce plasmonically-active substrates used for SERS applications, which is a non-destructive and reliable spectroscopy method, have been tried in recent years. Here we have presented an economical and easy procedure for synthesizing Ag NSs on Cu-grid in one step. Structural and elemental characterizations of Ag NSs on the Cu-grid were performed by scanning electron microscopy (SEM), energy-dispersive X-ray spectroscopy (EDX), X-ray diffraction (XRD), and X-ray photoelectron spectroscopy (XPS). Ag NSs on Cu-grids cause a high electromagnetic increase due to having complex morphology. Thus, the determination of R6G is easily realized even at very low concentrations such as 100 pM. It is predicted that different metallic nanostructures can be obtained by applying a similar recipe for different applications.

Keywords: Cu-grid, SERS, silver, rhodamine 6G.

1. Introduction

In recent years, surface-enhanced Raman spectroscopy (SERS) has been widely used in many fields such as chemistry, physics, materials science, and life science, as it is ultra-sensitive, dependable, has no labeling, and a non-destructive spectroscopic technique [1-3]. The developed SERS-active substrates are expected to be produced economically and efficiently, show high sensitivity, and are easy to use. SERS-active solid substrates are generally obtained using lithography and PVD [4-7]. While these production methods consist of long processing steps, they also require expensive and complex devices.

Chemical synthesis methods are a more straightforward and economical option for producing SERS-active materials. It is also possible to obtain more complex and off-hand structures that cause high electromagnetic field concentration. When using colloidal nanoparticles, it would be more appropriate to grow nanostructures in situ on the surface to avoid agglomeration, adversely affecting SERS measurements, and reusable if necessary. For this purpose, varied materials such as Si wafer, Al or Cu foil, and paper were used as solid substrates [8-11]. Silver and gold dendrites produced on commercial Al foil by galvanic replacement route were used as SERS-active substrates [12]. Similarly, Ag/Cu₂O heterostructures

synthesized on Cu foil by the hydrothermal synthesis method were evaluated to determine p-amino thiophenol and 4-pyridinethiol [13]. ZnO nanorods attached to the filter paper were modified with Au nanoparticles by UV-irradiation, and a reusable SERS-active substrate was obtained [14]. These studies showed that chemical synthesis methods could be exercised as high-activity SERS substrates when using plasmonic nanostructures on solid substrates.

Efficaciously, the Cu-grid is utilized to visualize the morphology of nanostructures with electron microscopy. Apart from this purpose, Gao et al. deposited Ag nanodendrites on Cu-grid by electrochemical deposition method and exerted for glucose determination [15]. Dendritic structured Ag nanocrystals on the Cu-grid were obtained with galvanic replacement by immersing in AgNO₃ solution [16]. In another study, the chemically synthesized Ag colloidal solution was dripped onto the Cu-grid and applied as SERS active substrate [17]. Even the silver nanoparticles grafted Ge nanowires were grown onto Cu-grid to achieve the detection limit of 6-aminopenicillins acid and penicillin G [18].

This study obtained Ag nanostructures (NSs) in a single step on the Cu-grid without any preliminary or device. These Ag nanostructures with sharp edges caused a severe enhancement of the electromagnetic field on the

surface and provided the opportunity to determine even very low concentrations of R6G. This procedure can also be performed for the in-situ growth of other metallic nanostructures.

2. Materials and Methods

2.1. Chemicals and Materials

Carbon-coated Cu-grid (400 mesh) was obtained from Electron Microscopy Science. Silver nitrate (AgNO_3 , $M_n=169.87$ g/mol), hydroquinone (HQ, $\text{C}_6\text{H}_6\text{O}_2$, $M_n=110.11$ g/mol), rhodamine 6G (R6G; $\text{C}_{28}\text{H}_{31}\text{N}_2\text{O}_3\text{Cl}$, $M_n=479.01$ g/mol) were purchased from Sigma-Aldrich. All aqueous solutions were prepared by using distilled water.

2.2. Fabrication of Ag NSs on the Cu-grid

In order to grow Ag NSs on Cu-grid, a fresh solution consisting of 0.2 mM AgNO_3 and 0.2 mM HQ in 50 mL of distilled water was prepared. First, the Cu-grids were cleaned with distilled water under sonication for 5 min. The cleaned Cu-grid was thrown into the solution and stirred at certain intervals (0.5, 1, and 2 hours) on the same experimental condition in the dark. Afterward, the Cu-grid removed from the solution was washed with distilled water and left to dry under room conditions.

2.3. Characterizations

The morphology and elemental analysis of Ag NSs on the Cu-grid were performed by scanning electron microscopy (SEM, ZEISS EVO LS10) and energy-dispersive X-ray spectroscopy (EDX, Bruker) attached with SEM at 25 keV. The crystal structure of Ag NSs was operated by an X-ray thin film diffractometer (Rigaku SmartLab) at 40 kV, 30 mA using $\text{Cu K}\alpha$ ($\lambda=0.154$ nm) radiation source. The chemical characterization of Ag NSs was conducted by X-ray photoelectron spectroscopy (XPS, SpecsFlex) using XR 50 M source exciting radiation.

SERS measurements were studied by a confocal Raman microscope (WITec Alpha 300 M+) with a 532 nm laser with a 50x objective (NA=0.85). The power of the laser was adjusted to 3 mW. 100 μM , 100 nM, and 100 pM of R6G solution with water as the probe molecule were prepared for the measurement. Each solution was dropped onto Ag NSs separately and left to dry at room temperature. After drying, SERS measurements were taken over 80x80 μm of area.

The analytical enhancement factor (AEF) was calculated by using the following equation (1) [19]:

$$AEF = \frac{I_{SERS}/C_{SERS}}{I_{Raman}/C_{Raman}} \quad (1)$$

Here, the concentrations of R6G dropped on only Cu-grid and Ag NSs are C_{Raman} and C_{SERS} , respectively. The peak

intensities at 1507 cm^{-1} of the Raman spectra obtained on these surfaces are I_{Raman} and I_{SERS} .

3. Results and Discussion

This study aims to procure plasmonically-active Ag NSs on a solid substrate without any seed in the medium. In Fig. 1, a schematic representation shows how to obtain Ag NSs grown on the carbon-coated Cu-grid. Here, a carbon-coated Cu-grid was added to the distilled water solution consisting of HQ as a reducing agent and, AgNO_3 as metal salt and stirred for two hours in a dark environment. Then, it was washed with distilled water and allowed to dry at room temperature. After this process, it was observed that Ag NSs grew successfully in large areas on the Cu-grid.

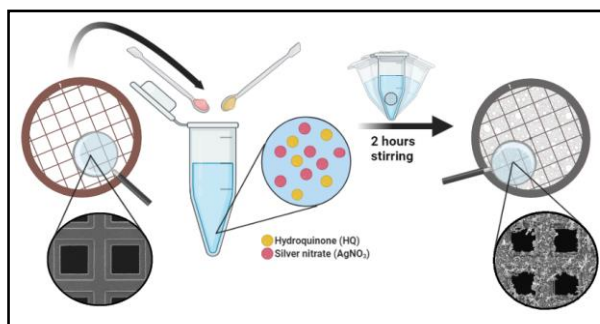


Figure 1. Schematic diagram of fabricating Ag NSs on Cu grid.

The commercially purchased Cu-grid surface is almost smooth in the SEM image (Fig. 2a). It can be an ideal solid substrate for growing Ag NSs without any seed. As shown in EDX analysis of the carbon-coated Cu-grid, although it contains mainly Cu (86.16 %) and relatively C (9.02 %) elements, trace amounts of O (2.58 %) and Al (2.24 %) elements are seen (Fig. 2b).

SEM pictures were taken to see the morphology of Ag NSs that we expect to grow on the Cu-grid after being kept in the appropriate solution medium. In Fig. 3a, it is seen that Ag NSs grow on almost the entire Cu-grid. There is no trace of that smooth surface before Cu-grid growth looking closer at the structures. The grid is wholly covered with Ag NSs (Fig. 3b). While there were nanoplates with smaller formations on the ground, especially the edges of the grid played a more active role, and a more intense Ag growth took place. Since the boundary lines have higher surface energy, reducing Ag ions in these regions is likely denser. For this reason, we come across the existence of highly symmetrical needle-like Ag NSs at the grid edges.

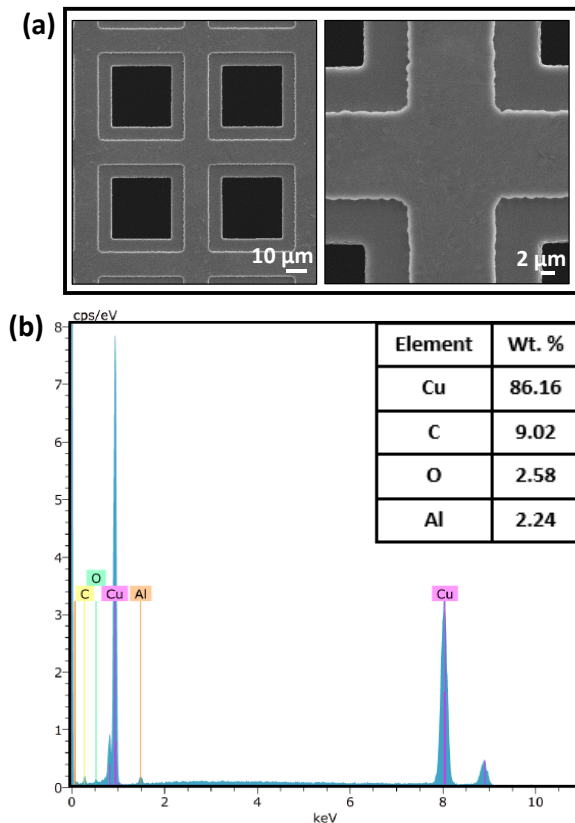


Figure 2. (a) SEM images of the Cu-grid. (b) EDX analysis of the Cu-grid.

In processes where the thermodynamic mechanism is dominant, crystals prefer to grow with a minimum total interfacial free energy. However, in cases where the kinetic mechanism dominates the thermodynamic

mechanism, it is expected to occur in different complex morphologies such as plate and needle-like, just like here. In this study, if the Cu grid in the growth solution is not shaken, there is no intense growth on the surface, as seen in Fig. 3c, and spherical particles tend to form rather than complex structures such as needles. We have also confirmed with the study that stirring is an important parameter affecting the growth mechanism [20].

The chemical composition of Ag NSs on the Cu-grid was characterized by EDX analysis and mapping. The Cu-grid at the base is symbolized with red, while the Ag NSs growing on it are marked with green in Fig. 4a. It is seen from the green color distribution that Ag NSs have grown successfully on the Cu-grid. When the EDX analysis is examined (Fig. 4b), the characteristic peak of Ag observed around 3 keV confirms that Ag NSs grew at a rate of 47.62% on the grid. The crystal structure of Ag NSs was examined with XRD analysis (Fig. 4c). Here, characteristic peaks of Cu at the bottom dominate, and Ag peaks are highly extinguished. The diffractions of (111), (200), and (220) planes of face cubic crystal (fcc) structured metallic Cu have peaks at 43.25°, 50.36°, and 74.06°, respectively. (JCPDS 85-1326). However, the peak around 38.02° belongs to the (111) plane diffraction of the fcc structured metallic Ag (JCPDS 87-0717). Since crystal growth of Ag is dominant in the (111) plane direction, only this peak can be observed. The XPS analysis of Ag NSs was given in Fig. 4d to characterize the chemical composition of Ag NSs further. It exhibited the characteristic peaks over Ag 3d region, which were split into 5/2, and 3/2 states at 367, and 373 eV, respectively. All structural and chemical characterizations support the growth of Ag NSs on the Cu-grid.

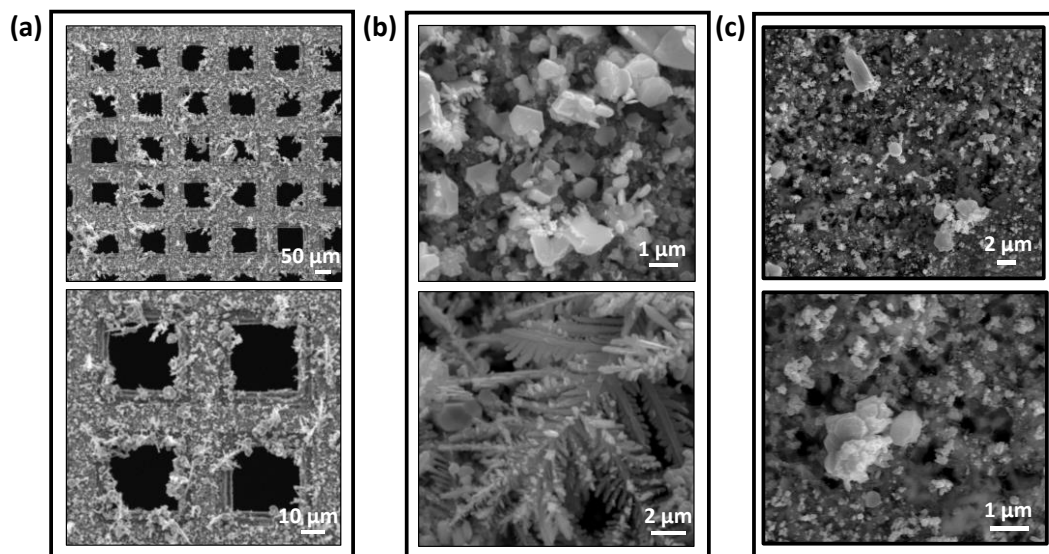


Figure 3. (a-b) SEM images of Ag NSs on Cu-grid at different magnifications. (c) SEM images of Ag NSs on Cu-grid without stirring.

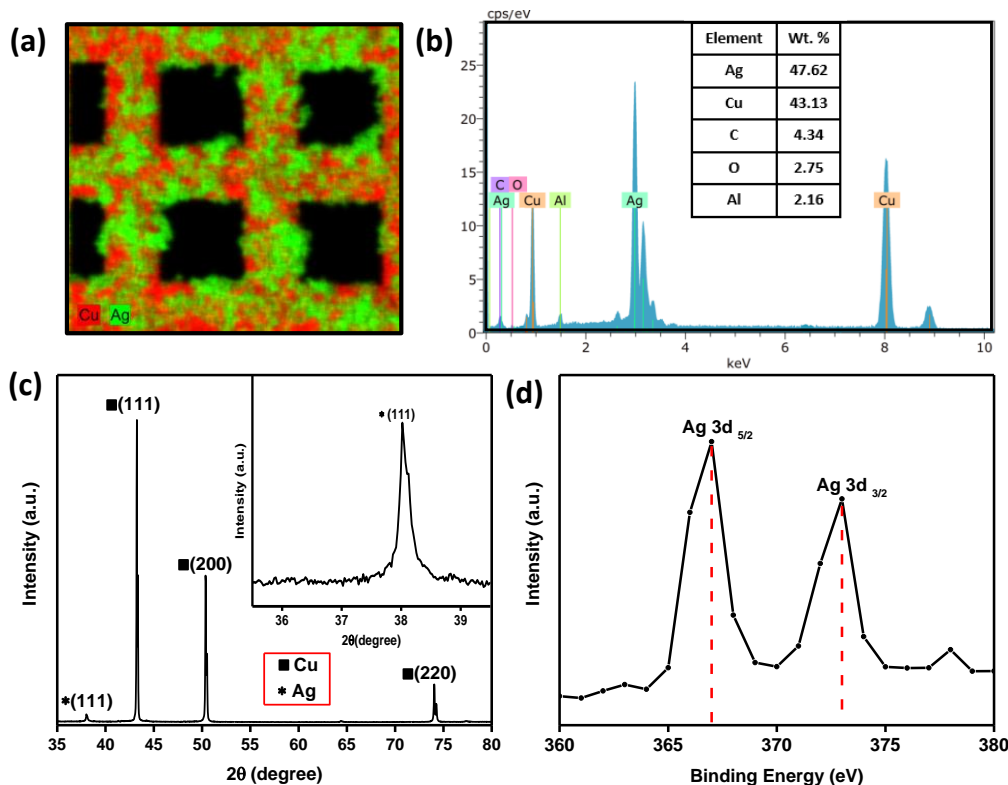


Figure 4. (a) EDX mapping and (b) EDX analysis (c) XRD analysis, and (d) XPS analysis of Ag NSs on the Cu-grid.

The growth of Ag NSs on the Cu-grid requires time. If we keep the reaction time at 0.5 hours (Fig. 5.a), we can see that Ag^{+1} ions are reduced on the Cu-grid, and nucleation begins. At this stage, the particles are relatively spherical and cover the entire surface. When the reaction is continued for 1 hour (Fig. 5.b), the particles grow more, go out of the spherical form, and nanoplates begin to form on the surface. Even needle-like structures are just starting to appear. When the time is completed to two hours, the existence of more complex shaped particles and needle-like structures that allow hot-spot formation becomes possible. According to the results of EDX analysis, it is seen that Ag formation on the surface increases with time (Fig. 5 c-d).

It is known that nanostructures with sharp corners and edges increase the number of hot spots on the surface, resulting in a higher Raman signal [21]. The branched hierarchical nanostructures and complex-shaped nanoparticles we see in Fig. 3b cause the electromagnetic field to intensity on the surface, positively affecting the SERS results. We can observe this clearly in Fig. 6a. Although Cu is a plasmonically-active material [22], since the surface of the Cu-grid is relatively smooth, we obtain a very low Raman signal even from the 100 μM of R6G solution on the Cu-grid. Thanks to the Ag NSs on the Cu-grid, we can get a very high Raman signal from the 100 μM of R6G solution.

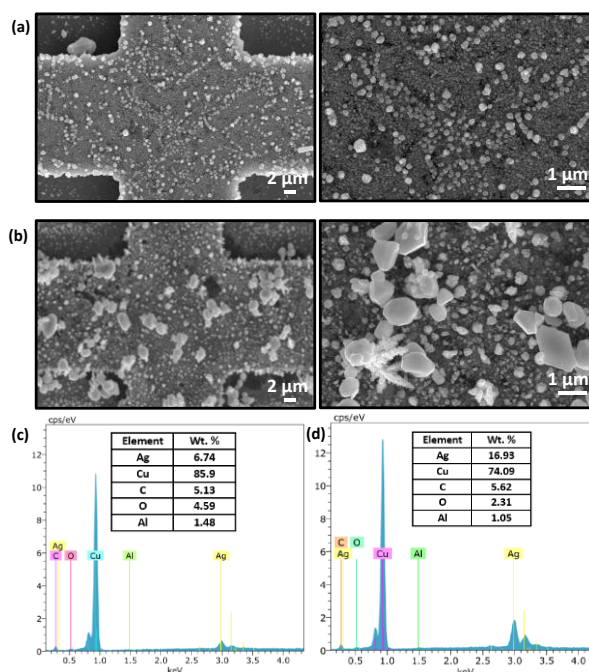


Figure 5. SEM images of Ag NSs on the Cu-grid after (a) 0.5, and (b) 1 hour. EDX analysis of (c) 0.5, and (d) 1 hour.

In Fig. 6b, there is Raman mapping filtered according to the band at 1507 cm^{-1} , which we have taken from the $100\text{ }\mu\text{M}$ of R6G solution on the Ag NSs. Here, we acquire a strong Raman signal over almost the entire area. The solutions prepared at lower concentrations were dropped on the Ag NSs to evaluate the limit of detection (LOD) of the R6G as a probe molecule. We can clearly distinguish the characteristic peaks of R6G at 612 cm^{-1} (C-C-C ring in-plane), 773 cm^{-1} (C-H out-of-plane), 1185 cm^{-1} (C-H in-plane); 1310 , 1363 , 1507 , 1575 , 1648 cm^{-1} (C-C stretching of the aromatic ring) even at a concentration as low as 100 pM (Fig. 6c) [23]. It is very valuable to fabricate a strong SERS substrate for ultra-trace sensing using a one-step, straightforward, low-cost method.

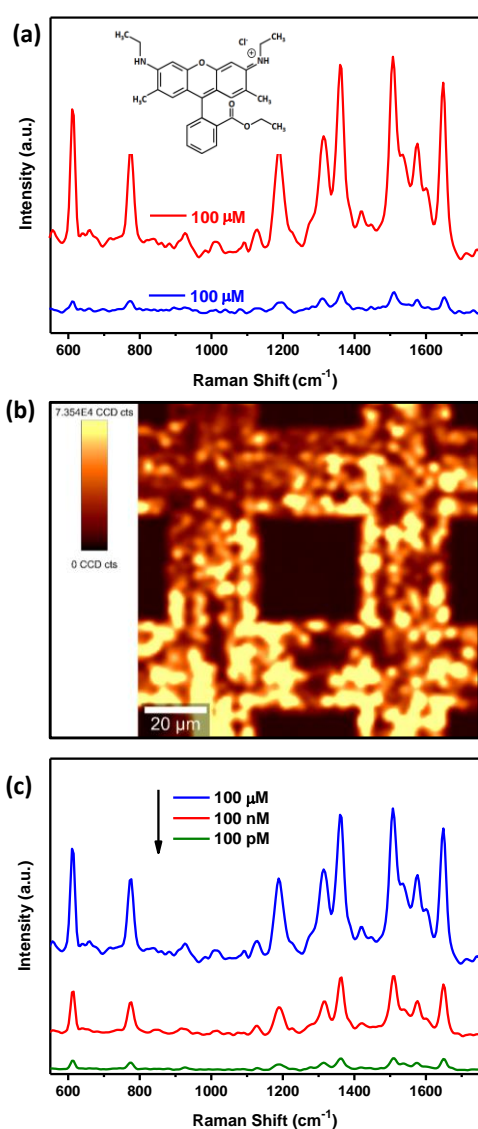


Figure 6. (a) SERS of R6G taken on Ag NSs (red line) and Cu-grid (blue line) (Inset: The chemical formula of R6G molecule). (b) SERS mapping of R6G on Ag NSs.

filtered with respect to the band at 1507 cm^{-1} . (c) Limit of detection of R6G on Ag NSs.

To calculate the AEF, we use the peak intensities at 1507 cm^{-1} of the Raman spectra in Fig. 6a. The peak intensities obtained from $100\text{ }\mu\text{M}$ of R6G solution dropped only on Cu-grid, and 100 pM of R6G solution dropped on Ag NSs are 206 and 193, respectively. When we replace these values in Formula (1), AEF is calculated as high as 9.37×10^6 . This result is quite remarkable compared to similar studies in the literature [15, 17].

4. Conclusion

The SERS-active substrate with a high enhancement factor of 9.37×10^6 has been fabricated using a simple, cheap, and one-step method for ultra-trace sensing applications. This method synthesized needle-like and complex-shaped Ag NSs, causing this superior enhancement in situ on Cu-grid to detect R6G as a probe molecule. Growing nanostructures in situ also avoid the agglomeration problem, which we often encounter in colloidal nanoparticles, and thus, many hot spots are formed with suitable nano-gaps. Herein, we have demonstrated that Ag NSs can be grown in situ on commercially available Cu-grids and be used as a SERS-active substrate. This method can also be applied to grow other metallic nanostructures for different applications.

Author's Contributions

Menekşe Şakir: Drafted and wrote the manuscript, performed the experiment and result analysis.

Ethics

There are no ethical issues after the publication of this manuscript.

References

- [1] Mosier-Boss, P. A. 2017. Review of SERS substrates for chemical sensing. *Nanomaterials*; 7(6): 142.
- [2] Sharma, B., Frontiera, R. R., Henry, A.-I., Ringe, E., Van Duyne, R. P. 2012. SERS: Materials, applications, and the future background and mechanism. *Materials Today*; 15(1-2): 16-25.
- [3] Sharma, B., Fernanda Cardinal, M., Kleinman, S. L., Greeneltch, N. G., Frontiera, R. R., Blaber, M. G., Schatz, G. C., Van Duyne, R. P. 2013. High-performance SERS substrates: Advances and challenges. *MRS Bulletin*; 38(8): 615–624.
- [4] Green, M., Liu, F. M. 2003. SERS substrates fabricated by island lithography: The silver/pyridine system. *Journal of Physical Chemistry B*; 107(47): 13015–13021.
- [5] Nowicka, A. B., Czaplicka, M., Kowalska, A. A., Szymborski, T., Kamińska, A. 2019. Flexible PET/ITO/Ag SERS platform for label-free detection of pesticides. *Biosensors*; 9(3): 111.
- [6] Suresh, V., Ding, L., Chew, A. B., Yap, F. L. 2018. Fabrication of large-area flexible SERS substrates by nanoimprint lithography. *ACS Applied Nano Materials*; 1(2): 886–893.

- [7]. Xu, B. B., Zhang, Y. L., Zhang, W. Y., Liu, X. Q., Wang, J. N., Zhang, X. L., Zhang, D. D., Jiang, H. B., Zhang, R., Sun, H. B. 2013. Silver-coated rose petal: Green, facile, low-cost and sustainable fabrication of a SERS substrate with unique superhydrophobicity and high efficiency. *Advanced Optical Materials*; 1(1): 56–60.
- [8]. Fodjo, E. K., Li, D. W., Marius, N. P., Albert, T., Long, Y. T. 2013. Low temperature synthesis and SERS application of silver molybdenum oxides. *Journal of Materials Chemistry A*; 1(7): 2558–2566.
- [9]. Fu, J., Ye, W., Wang, C. 2013. Facile synthesis of Ag dendrites on Al foil via galvanic replacement reaction with $[\text{Ag}(\text{NH}_3)_2]\text{Cl}$ for ultrasensitive SERS detecting of biomolecules. *Materials Chemistry and Physics*; 141(1): 107–113.
- [10]. Korkmaz, I., Sakir, M., Sarp, G., Salem, S., Torun, I., Volodkin, D., Yavuz, E., Onses, M. S., Yilmaz, E. 2021. Fabrication of superhydrophobic $\text{Ag@ZnO@Bi}_2\text{WO}_6$ membrane disc as flexible and photocatalytic active reusable SERS substrate. *Journal of Molecular Structure*; 1223: 129258.
- [11]. Yuan, J., Lai, Y., Duan, J., Zhao, Q., Zhan, J. 2012. Synthesis of a β -cyclodextrin-modified Ag film by the galvanic displacement on copper foil for SERS detection of PCBs. *Journal of Colloid and Interface Science*; 365(1): 122–126.
- [12]. Ye, W., Chen, Y., Zhou, F., Wang, C., Li, Y. 2012. Fluoride-assisted galvanic replacement synthesis of Ag and Au dendrites on aluminum foil with enhanced SERS and catalytic activities. *Journal of Materials Chemistry*; 22(35): 18327–18334.
- [13]. Ji, R., Sun, W., Chu, Y. 2014. One-step hydrothermal synthesis of $\text{Ag/Cu}_2\text{O}$ heterogeneous nanostructures over Cu foil and their SERS applications. *RSC Advances*; 4(12): 6055–6059.
- [14]. Sakir, M., Salem, S., Sanduvac, S. T., Sahmetlioglu, E., Sarp, G., Onses, M. S., Yilmaz, E. 2020. Photocatalytic green fabrication of Au nanoparticles on ZnO nanorods modified membrane as flexible and photocatalytic active reusable SERS substrates. *Colloids Surf. A*; 585: 124088.
- [15]. Gao, Y., Zhang, C., Yang, Y., Yang, N., Lu, S., You, T., Yin, P. 2021. A high sensitive glucose sensor based on Ag nanodendrites/Cu mesh substrate via surface-enhanced Raman spectroscopy and electrochemical analysis. *J. Alloys Compd.*; 863: 158758.
- [16]. Guo, T. L., Li, J. G., Sun, X., Sakka, Y. 2016. Improved galvanic replacement growth of Ag microstructures on Cu micro-grid for enhanced SERS detection of organic molecules. *Mater. Sci. Eng. C*; 61: 97–104.
- [17]. Sharma, H. S. S., Carmichael, E., McCall, D. 2016. Fabrication of SERS substrate for the detection of rhodamine 6G, glyphosate, melamine and salicylic acid, *Vibrational Spectroscopy*; 83: 159–169.
- [18]. Zhou, Q., Meng, G., Liu, J., Huang, Z., Han, F., Zhu, C., Kim, D. J., Kim, T., Wu, N. 2017. A hierarchical nanostructure-based surface-enhanced Raman scattering sensor for preconcentration and detection of antibiotic pollutants. *Adv. Mater. Technol.*; 2(6): 1700028.
- [19]. Salem, S., Sakir, M., Sahin, K., Korkmaz, I., Yavuz, E., Sarp, G., Onses, M. S., Yilmaz, E. 2020. Low bandgap microsphere-like magnetic nanocomposite: An enhanced photocatalyst for degradation of organic contaminants and fabrication of SERS-active surfaces. *Colloids Surf. A*; 589: 124436.
- [20]. Sakir, Menekse, Yilmaz, E., Onses, M. S. 2020. SERS-active hydrophobic substrates fabricated by surface growth of Cu nanostructures. *Microchemical Journal*; 154: 104628.
- [21]. Sakir, Menekse, Pekdemir, S., Karatay, A., Küçüköz, B., Ipekci, H. H., Elmali, A., Demirel, G., Onses, M. S. 2017. Fabrication of plasmonically active substrates using engineered silver nanostructures for SERS applications. *ACS Applied Materials and Interfaces*; 9(45): 39795–39803.
- [22]. Cejkova, J., Prokopec, V., Brazdova, S., Kokaislova, A., Matejka, P., Stepanek, F. 2009. Characterization of copper SERS-active substrates prepared by electrochemical deposition. *Applied Surface Science*; 255(18): 7864–7870.
- [23]. Zang, L. S., Chen, Y. M., Koc-Bilican, B., Bilican, I., Sakir, M., Wait, J., Çolak, A., Karaduman, T., Ceylan, A., Ali, A., Elbuken, C., Serdar Onses, M., Kaya, M. 2021. From bio-waste to biomaterials: The eggshells of Chinese oak silkworm as templates for SERS-active surfaces. *Chemical Engineering Journal*; 426: 131874.